

NRL Report 8868

Full Field Ambiguity Function Processing in a Complex Shallow-Water Environment

R. M. HEITMEYER

*SACLANT ASW Research Centre
La Spezia, Italy*

R. G. FIZELL AND W. B. MOSELEY

*Applied Ocean Acoustics Branch
Acoustics Division*

December 31, 1984



NAVAL RESEARCH LABORATORY
Washington, D.C.

Approved for public release; distribution unlimited.

SECURITY CLASSIFICATION OF THIS PAGE

REPORT DOCUMENTATION PAGE				
1a. REPORT SECURITY CLASSIFICATION UNCLASSIFIED		1b. RESTRICTIVE MARKINGS		
2a. SECURITY CLASSIFICATION AUTHORITY		3. DISTRIBUTION / AVAILABILITY OF REPORT		
2b. DECLASSIFICATION / DOWNGRADING SCHEDULE		Approved for public release; distribution unlimited.		
4. PERFORMING ORGANIZATION REPORT NUMBER(S) NRL Report 8868		5. MONITORING ORGANIZATION REPORT NUMBER(S)		
6a. NAME OF PERFORMING ORGANIZATION Naval Research Laboratory	6b. OFFICE SYMBOL (If applicable)	7a. NAME OF MONITORING ORGANIZATION		
6c. ADDRESS (City, State, and ZIP Code) Washington, DC 20375-5000		7b. ADDRESS (City, State, and ZIP Code)		
8a. NAME OF FUNDING / SPONSORING ORGANIZATION Office of Naval Research	8b. OFFICE SYMBOL (If applicable)	9. PROCUREMENT INSTRUMENT IDENTIFICATION NUMBER		
8c. ADDRESS (City, State, and ZIP Code) Arlington, VA 22217		10. SOURCE OF FUNDING NUMBERS		
		PROGRAM ELEMENT NO. RR011-08-43	PROJECT NO. 61153N	WORK UNIT ACCESSION NO. DN280-034
11. TITLE (Include Security Classification) Full Field Ambiguity Function Processing in a Complex Shallow-Water Environment				
12. PERSONAL AUTHOR(S) Heitmeyer,* R.M., Fizell, R.G., and Moseley, W.B.				
13a. TYPE OF REPORT Interim	13b. TIME COVERED FROM _____ TO _____	14. DATE OF REPORT (Year, Month, Day) 1984 December 31	15. PAGE COUNT 21	
16. SUPPLEMENTARY NOTATION *SACLANT ASW Research Centre La Spezia, Italy				
17. COSATI CODES		18. SUBJECT TERMS (Continue on reverse if necessary and identify by block number)		
FIELD	GROUP	SUB-GROUP	Acoustic fields Normal-mode theory	
			Ambiguity function processing Pekeris channel	
			Array resolution Source localization	
19. ABSTRACT (Continue on reverse if necessary and identify by block number)				
<p>For many acoustic environments, the power in a target's acoustic field incident on a linear array segment is concentrated in horizontal angle but distributed over a significant vertical angle. For these environments, both signal-to-noise ratio (S/N) gains and range, bearing, and depth estimates may be possible from an "ambiguity surface processor" obtained as a spatial correlation using a replica of the signal field in the three unknown source location parameters. This report presents an initial evaluation of an ambiguity surface processor for the Pekeris acoustic environment. Results for a vertical array segment indicate high-quality estimates of both range and depth. For a segment with horizontal extent and for known source depth, the sharp main peak of the ambiguity surface also supports high-quality estimates of source range and bearing, although for small array tilt angles, the quality of the range estimate is limited by the prevailing S/N because of the presence of extraneous sidelobe peaks. Increasing the tilt angle significantly reduces the level of the sidelobe peaks. Furthermore, the ambiguity surface processor achieves gain enhancements up to 2 dB using a purely horizontal array, and in excess of 20 dB using the vertical array.</p>				
20. DISTRIBUTION / AVAILABILITY OF ABSTRACT <input checked="" type="checkbox"/> UNCLASSIFIED/UNLIMITED <input type="checkbox"/> SAME AS RPT <input type="checkbox"/> DTIC USERS		21. ABSTRACT SECURITY CLASSIFICATION UNCLASSIFIED		
22a. NAME OF RESPONSIBLE INDIVIDUAL Richard G. Fizell		22b. TELEPHONE (Include Area Code) (202) 767-2192	22c. OFFICE SYMBOL 5120	

DD FORM 1473, 84 MAR

83 APR edition may be used until exhausted.

All other editions are obsolete.

SECURITY CLASSIFICATION OF THIS PAGE

CONTENTS

INTRODUCTION	1
AMBIGUITY FUNCTION PROCESSING	2
ACOUSTIC ENVIRONMENT	3
PERFORMANCE EXAMPLES	8
CONCLUSIONS AND RECOMMENDATIONS	13
ACKNOWLEDGMENTS	14
APPENDIX A – Maximum Array Gain Value	15
APPENDIX B – Modal Functions, Horizontal Wavenumber Components, and the Number of Modes	16
APPENDIX C – Impossibility of Resolving Vertical Arrival Structure	17

FULL FIELD AMBIGUITY FUNCTION PROCESSING IN A COMPLEX SHALLOW-WATER ENVIRONMENT

INTRODUCTION

Conventional beamforming is based on the premise that the incident acoustic power from a point source consists of a single planewave arrival or, at most, is concentrated in a few *near planewave* arrival groups. When the signal consists of a single planewave arrival, and when the noise is spatially uncorrelated and Gaussian, the conventional beamformer constitutes a generalized likelihood ratio detector and a maximum likelihood estimator of the arrival angle. In this context, the conventional beamformer can be viewed as the spatial correlation of the observed acoustic field with a planewave replica, computed as a function of the unknown planewave arrival angle.

For many acoustic environments, however, the incident acoustic power may be concentrated in horizontal angle, but distributed over a significant sector in vertical angle. When this is the case, significant degradation in both detection performance and angle estimation can result with conventional beamforming, particularly for arrays with vertical extent, or for horizontal arrays with the signal field incident in a direction near endfire. For these environments, it may be possible not only to improve detection performance, but to estimate the range, bearing, and depth of a source by using an accurate replica of the signal field for the spatial correlation, rather than the planewave replica. The output of the resultant spatial processor can be viewed as an ambiguity surface in the unknown source location parameters, from which both detection and source location estimates are made.

Two issues are basic to a potential application of an ambiguity function processor. First, for what acoustic environments, if any, is the performance improvement sufficient to warrant the detailed environmental knowledge and the computational complexity required to implement the processor? A likely candidate is an acoustic field with a complex vertical arrival structure, since it is the vertical arrival structure that will determine the quality of the source location estimates. Furthermore, a complex arrival structure can also cause severe gain degradation for the conventional beamformer, and thus the added complexity may be justified to achieve acceptable detection performance. Secondly, how does the performance depend on the orientation of the array segment? A vertical array cannot provide a bearing estimate, but it should provide the best estimate of source depth with an ambiguity function processor, since it is best able to utilize the vertical arrival structure. Furthermore, the vertical array with conventional beamforming suffers the most signal gain degradation. In contrast, a horizontal array should provide the best estimate of source bearing, but the worst estimate of source depth. Moreover, at least for source bearings near broadside, there should be only modest signal gain degradation, for the case of conventional beamforming. This report presents an analytic performance evaluation of the full field ambiguity function processor for a specific acoustic environment with a highly complex vertical arrival structure. In the second section of this report, the ambiguity function processor is defined for an arbitrary acoustic environment, and its basic properties are established. In this section, an *array gain enhancement* factor is defined to provide a quantitative measure of the improvement in signal-to-noise ratio (S/N) relative to the planewave beamformer. In the third section, the acoustic environment is restricted to the so-called *Pekeris channel*, which is representative of certain shallow water areas. In the associated appendixes of this report it is shown that for this environment, it is not possible to resolve the incident vertical arrival structure with conventional beamforming. The fourth section of this report

presents specific examples of both the ambiguity surface and the array gain enhancement factor for selected vertical array orientations, source bearings, and source ranges. And the fifth section summarizes the results and identifies certain key issues requiring further analysis.

AMBIGUITY FUNCTION PROCESSING

We assume that the acoustic environment is sufficiently well known that it is possible to compute an estimated *replica* of the pressure field at each hydrophone as a function of the unknown source location parameters, $P'_s = (R'_s, \theta'_s, Z'_s)$. When this is the case, and when the noise is Gaussian and spatially uncorrelated, both the optimum generalized likelihood ratio detector and the maximum likelihood estimator of the source location parameters can be obtained by spatially correlating the observed pressure field with the replica field. In particular, we define the "source location ambiguity function," $A(P'_s; P_s)$, by

$$A(P'_s; P_s) = \left| \sum_n P_n(P_s) s_n^*(P'_s) \right|^2 / N \sum_n |s_n(P'_s)|^2, \quad (1)$$

where $P_s = (R_s, \theta_s, Z_s)$ are the true source location parameters, $p_n(P_s)$ is the pressure field observed at the n th hydrophone element, $s_n(P'_s)$ is the replica field, and "*" denotes complex conjugation. The detection condition is $A(P'_s; P_s) > T$, where T is the threshold value corresponding to a particular false alarm probability, and the source location parameter estimate, $\hat{P}_s = (\hat{R}_s, \hat{\theta}_s, \hat{Z}_s)$, is the value of P'_s that maximizes $A(P'_s; P_s)$. (The ambiguity function is seen to be similar, but not identical, to the "Detection Factor" of Bucker.¹)

The replica correlator processor has the property that it maximizes the S/N when the set of replica fields includes the observed pressure field. In particular, in Appendix A, it is shown that, with the array gain defined as

$$GA = GS/GN, \quad (2a)$$

where the signal gain is

$$GS = \max_{P'_s} \{A(P'_s; P_s)\} / (\sum |p_n|^2 / N), \quad (2b)$$

and the noise gain is

$$GN = E\{A | \text{noise only}\} / E\{|p_n|^2 | \text{noise only}\}, \quad (2c)$$

the array gain is

$$GA = N \quad (3)$$

when $P'_s = P_s$. Note that this is the same array gain as that obtained for the conventional beamformer when the signal field consists of a single planewave.

The conventional beamformer can be viewed as a special case of the replica correlator processor obtained by restricting the set of replica fields to the set of planewaves. This is seen by noting that, for a planewave, the replica is $s_n(\omega) = \exp[-i(2\pi/\lambda) \cdot \hat{\mu}(\omega) \cdot \hat{a}_n]$, where $\hat{\mu}(\omega)$ is a unit vector in the direction ω , and \hat{a}_n is the position vector to the n th hydrophone. Substituting into Eq. (1) yields

$$A_b(\omega, P_s) = \left| \sum p_n(P_s) \exp[i(2\pi/\lambda) \cdot \hat{\mu}(\omega) \cdot \hat{a}_n] \right|^2 / N^2, \quad (4)$$

¹H.P. Bucker, "Use of Calculated Sound Fields and Matched-Field Detection to Locate Sound Sources in Shallow Water," *J. Acoust. Soc. Am.*, **59**, 368 (1976).

which is recognized as the usual expression for a planewave beamformer. Note that the noise gain for spatially uncorrelated noise is $(1/N)$. Furthermore, if the pressure field can also be represented as a planewave, the signal gain is unity, and hence the array gain is N . When the pressure field is not a simple planewave, the signal gain,

$$GS_b = \max_{\omega} \left\{ \left| \sum p_n(P_s) \cdot \exp [i(2\pi/\lambda) \cdot \hat{\mu}(\omega) \cdot \hat{a}_n] \right|^2 \right\} / N \sum |p_n|^2, \quad (5)$$

is less than unity, and the array gain,

$$GA_b = N \cdot GS_b, \quad (6)$$

is less than N .

For a given acoustic environment, the ratio GA/GA_b provides a measure of the improvement in performance for the replica correlator relative to that of the conventional beamformer. This ratio, which we refer to as the array gain enhancement, GAE, represents the increase in the S/N obtained by using an accurate replica of the signal field, rather than the planewave replica assumed in conventional beamforming. From Eqs. (3) and (6), it is seen that GAE is numerically equal to $(1/GS_s)$.

ACOUSTIC ENVIRONMENT

Figure 1 illustrates the source-receiver geometry. We assume a linear array segment of length $(L-L/N)$, with N equally spaced hydrophone elements at spacing $d = L/N$, located in the H-V plane of the coordinate system H, V, B. The axes of the coordinate system are determined so that the horizontal axis, H, points in the direction of increasing hydrophone number, the vertical axis, V, points in the direction of decreasing water depth, and the broadside axis, B, is chosen to form a right-handed system. The midpoint of the array segment, which corresponds to the origin of the coordinate system, is located at depth Z_a , and the vertical tilt angle ϕ_a is measured from the H axis is indicated in Fig. 1. The source is located at range R_s , depth Z_s , and azimuth θ_s , measured relative to the broadside axis.

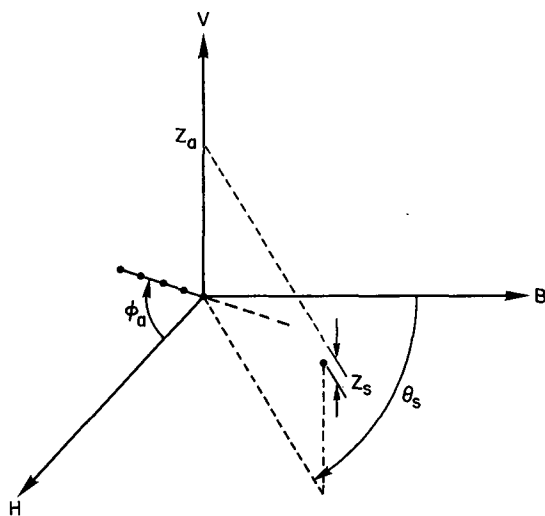


Fig. 1 — Geometry of source and array. Midpoint of array in at origin; array lies in H-V plane at angle ϕ_a to H-axis; water surface is Z_a above H-B plane; source is at depth Z_s below surface; projection of source on H-B plane is at angle θ_s to B-axis.

For stratified media with homogeneous layers, the complex pressure field at the n th hydrophone can be written in terms of a modal representation as

$$p_n(R_s, \theta_s, Z_s; r_n, z_n) = \sum_{m=1}^{M} U_m(z_s) \cdot U_m(z_n) \cdot \exp [iK_m r_n] / [K_m r_n]^{1/2}, \quad (7)$$

where $U_m(z)$ is the m th modal function, K_m is the horizontal component of the m th wavenumber vector, and M is the number of discrete modes. The depth of the n th hydrophone element, z_n , and the source range r_n , are given by

$$z_n = z_a + nd \cdot \sin(\phi_a) \quad (8a)$$

and

$$r_n = [(R_s \cdot \cos(\theta_s))^2 + (R_s \cdot \sin(\theta_s) + nd \cdot \cos(\phi_a))^2]^{1/2} \quad (8b)$$

for $n = -N_m, -N_m+1, \dots, N_m-1, N_m$, where $N_m = (M-1)/2$. Note that the source ranges for a source at $\theta'_s = 180 - \theta_s$ are the same as those for a source at θ_s . Furthermore, for a vertical array ($\phi_a = 90^\circ$) the source ranges are identically equal to R_s , and independent of θ_s . These relationships reflect the usual source-location ambiguities associated with a linear array segment.

The Pekeris channel consists of two layers, a water layer and a bottom layer, each with a sound speed and density that are independent of range, bearing, and depth. Let C_w and C_b be the sound speeds in the water and bottom layers, respectively, let ρ_w, ρ_b be the corresponding densities, and let H be the water depth. Then, if both the range and depth are expressed in terms of the wavelength λ , the functional form of the pressure will be determined by three parameters: the relative sound speed $c_r = (C_w/C_b)$, the relative density $\rho = (\rho_w/\rho_b)$, and the water depth, H , expressed in terms of wavelengths, H/λ . The equations specifying the modal functions, the horizontal wavenumber components, and the number of modes are contained in Appendix B.

Figure 2 shows the character of the acoustic field for a Pekeris channel in terms of the power (top plot) and the magnitude of the phase (bottom plot) for a segment of the range-depth plane. The illustrated field corresponds to a 60λ water depth, a relative sound speed of 0.95, and a relative density of 0.33. The source depth is $1/10$ th the water depth, or equivalently 6λ . The range interval is centered at 40 water depths (2400λ) and spans an interval of 6 water depths (360λ). These parameters are used for all the performance examples.

The complexity of the field illustrated in Fig. 2 can be attributed to the fact that, for each range point, the field is obtained as a linear combination of a large number of planewave arrivals whose vertical angles are both closely spaced and distributed over a large fraction of the full, 180° , vertical angle sector. In particular, in Appendix C it is shown that, for the Pekeris channel, the vertical arrival angles are so closely spaced that it is not possible to resolve individual arrivals with conventional beamforming on a vertical array, regardless of the length of the array. It is this complex vertical arrival structure that is exploited in the source localization estimate.

Figures 3 and 4 illustrate the field as seen on conventional arrays for arrays with 0° tilt (horizontal) and 90° tilt. Beam patterns are obtained for targets at fixed depths and bearings (irrelevant for the vertical array) and ranges vary over intervals from 37 to 43 times the channel depth, or 17 to 23 times the channel depth, as indicated; they are normalized to a maximum value of one for each surface, for display purposes.

For the horizontal array, the variation in the field across the aperture is caused only by the range dependence of the individual hydrophone in the array; this range dependence results primarily from both the variation in the phase across the aperture of each of the constituent cylindrical wave fronts

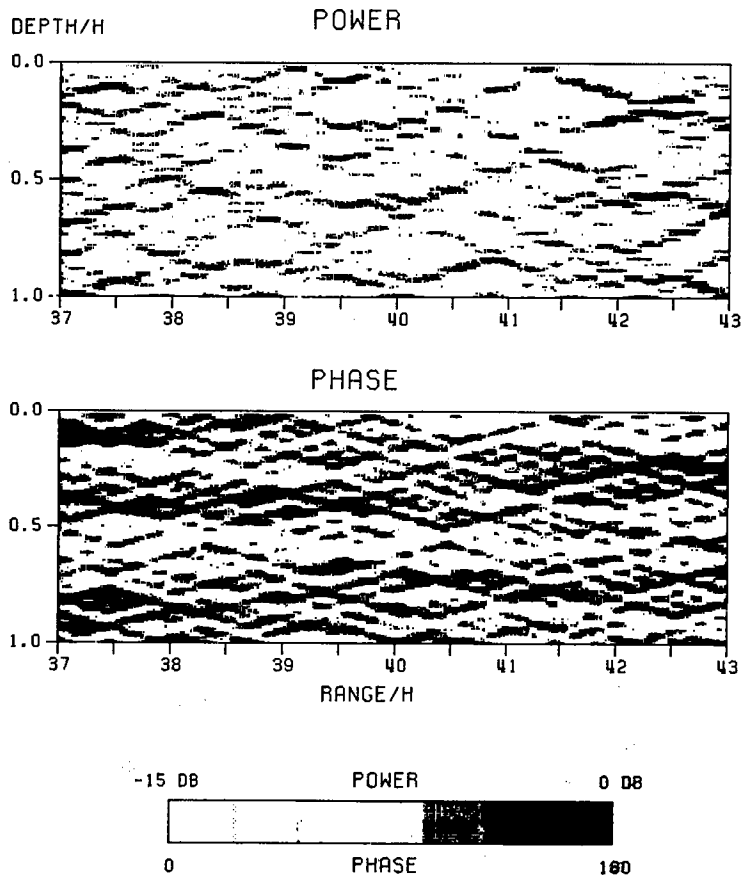


Fig. 2 — Power (top) and phase (bottom) at distances centered at 40 water depths from source. Water depth = 60λ ; source depth = 6λ ; relative sound speed = 0.95.

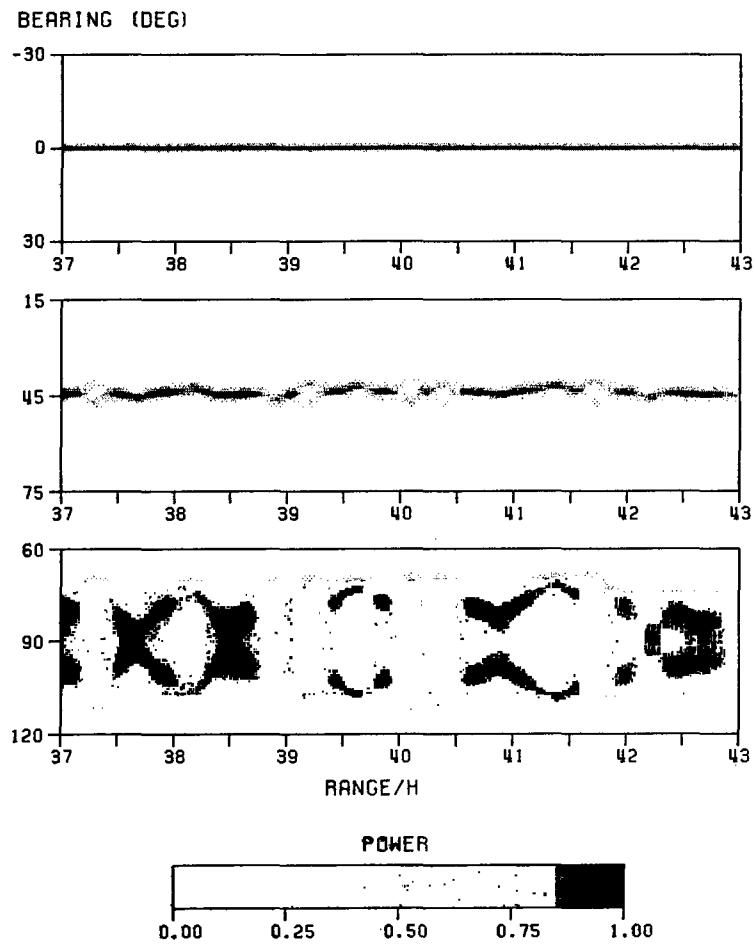


Fig. 3 — Conventional bearing response surfaces for horizontal array and sources with bearings fixed at 0° (top), 45° (middle), and 90° (bottom), depth fixed at 0.1 channel depths, and ranges varying from 37 to 43 channel depths

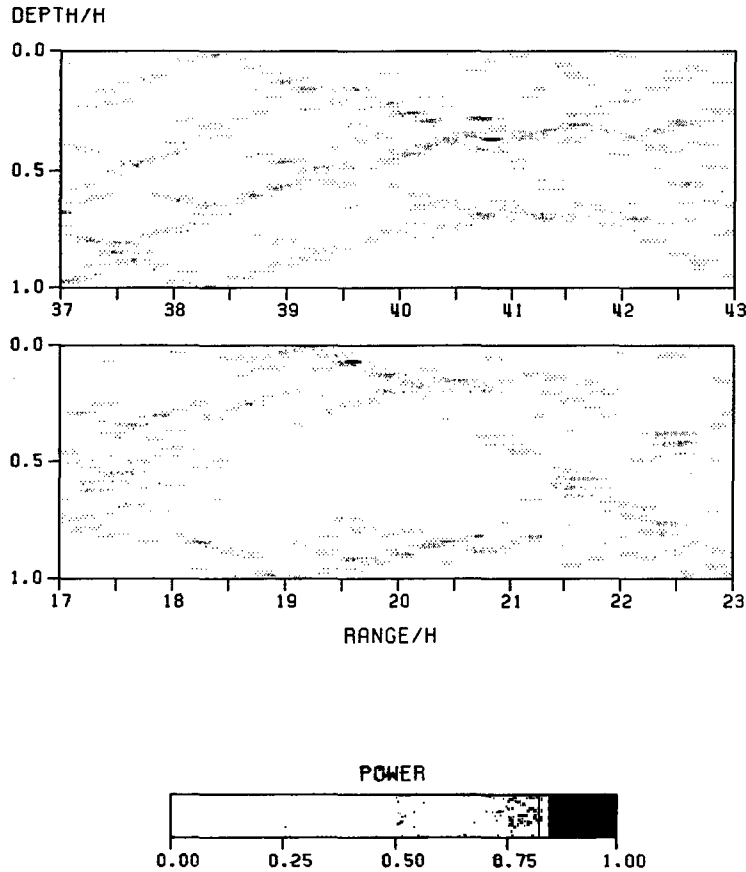


Fig. 4 — Conventional response surfaces for vertical array and sources with depth fixed at 0.1 channel depths and ranges varying from 37 to 43 channel depths (top) and 17 to 23 channel depths (bottom)

because of wave-front curvature and from the *multipath* effects associated with the coherent combination of these wave fronts to form the total field. For the source ranges used in this analysis the multipath effects are the dominant cause of the field variation, since the wave-front curvatures across the total aperture are almost negligible.

Figure 3 shows that the complex vertical field structure causes the conventional response surface to degrade significantly for targets off broadside; this degradation is exhibited in lower main peaks than those produced by planewave signals and in the presence of spurious peaks at bearings distinct from the actual target, for most values of the actual target range. The conventional beamformer response surface for the broadside target suffers a degradation of 0.006 dB in the array gain averaged over all source ranges. In this case, the array samples a negligible amount of the multipath structure. For the target at 45°, the array has a significant projection on the vertical plane containing the source (shown in Fig. 1) and begins to see some multipaths that tend to shift the beam response slightly toward broadside for most target ranges. When the beam response is averaged over all source ranges, the peak is shifted to 44°. The array gain degradation averaged over the indicated source ranges is 0.6 dB. For a target at endfire, the array lies in the vertical plane of the source; consequently, more of the multipath structure is seen. This shifts the conventional response pattern away from endfire for most source ranges; the range-averaged response has a peak displaced 10°, and the averaged array gain degradation is 0.815 dB.

Other calculations show that the array gain degradation becomes more pronounced both as array tilt angle increases and as target bearing moves further from broadside; in each case, more of the multipath character of the field is sampled by the array. These calculations were done for several array geometries, and these array gain degradations provided the array enhancement factors indicated on the ambiguity surfaces shown in Figs. 5 through 8 and in Table 1.

For the vertical array, the conventional response surface in Fig. 4 shows vertical angle beam patterns as the true source range varies over the indicated intervals. The complex modal field structure, as exhibited by vertical multipath structure, can be seen in Fig. 4 to be unresolvable by the conventional beamformer, as has been mentioned previously.

PERFORMANCE EXAMPLES

Here the performance of the ambiguity function processor is examined through direct computations of both the ambiguity surface and the array gain enhancement factor. The form of the ambiguity surface provides a qualitative measure of the source location error in terms of the sharpness of the peak at the true source location value and the extent to which extraneous peaks are introduced. The array gain enhancement factor quantifies the improvement in S/N relative to the conventional beamformer.

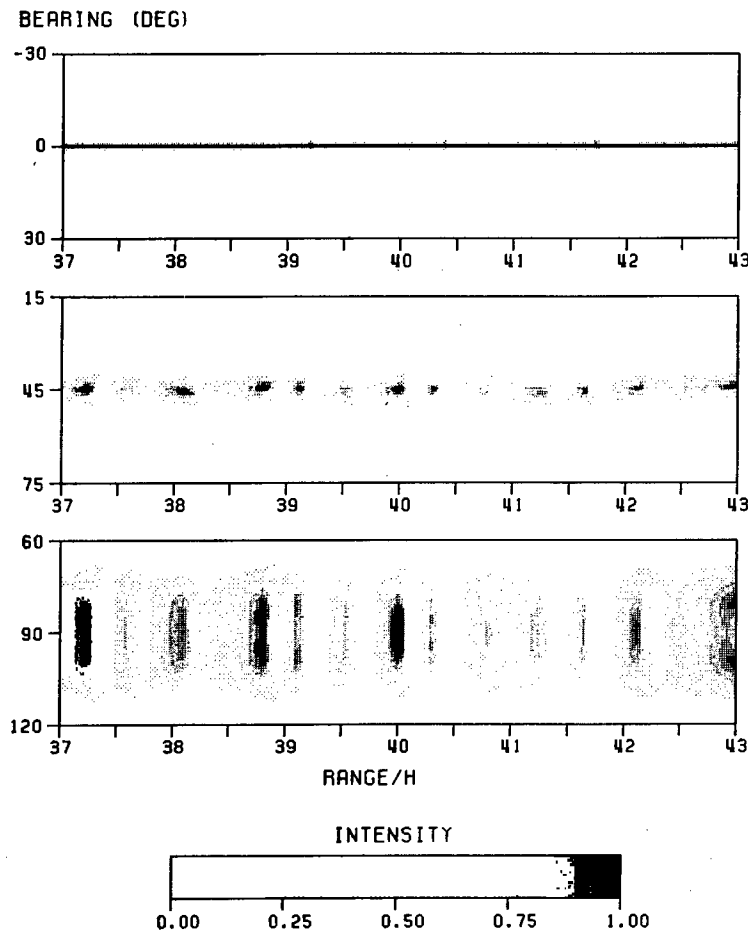


Fig. 5 — Range-bearing ambiguity surfaces for horizontal array. Three source bearings are 0° (top), 45° (middle), and 90° (bottom). (See text for other relevant parameters.) Array gain enhancement factors are 0.006 dB (top), 0.6 dB (middle), and 0.815 dB (bottom).

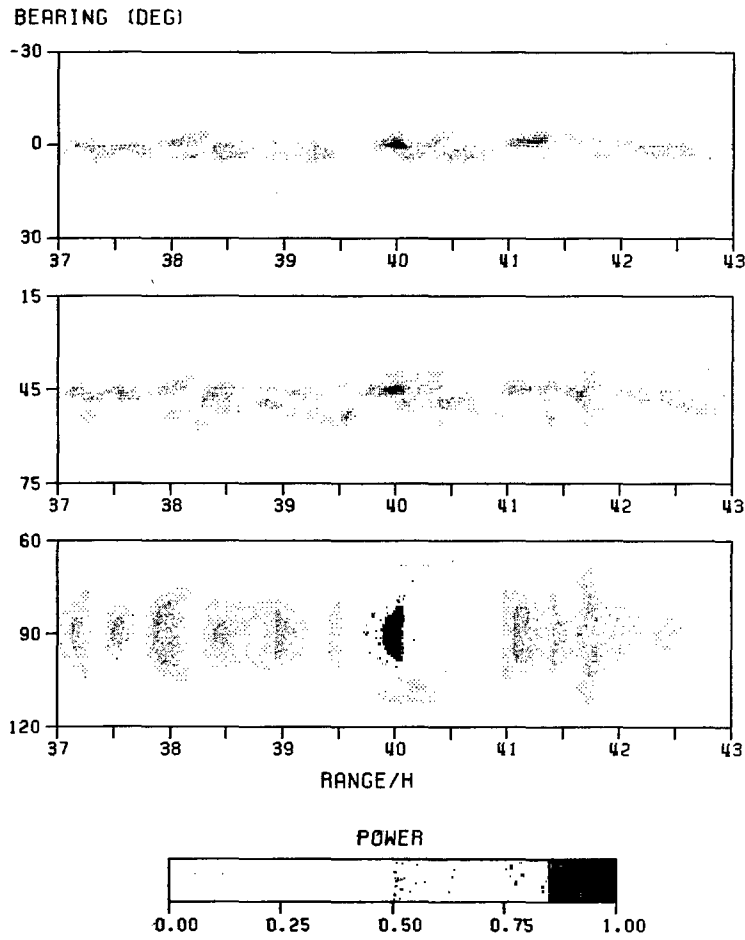


Fig. 6 — Range-bearing ambiguity surfaces for array with 10° tilt. Other parameters are as in Fig. 5. Array gain enhancement factors are 1.72 dB (top), 1.56 dB (middle), and 1.76 dB (bottom).

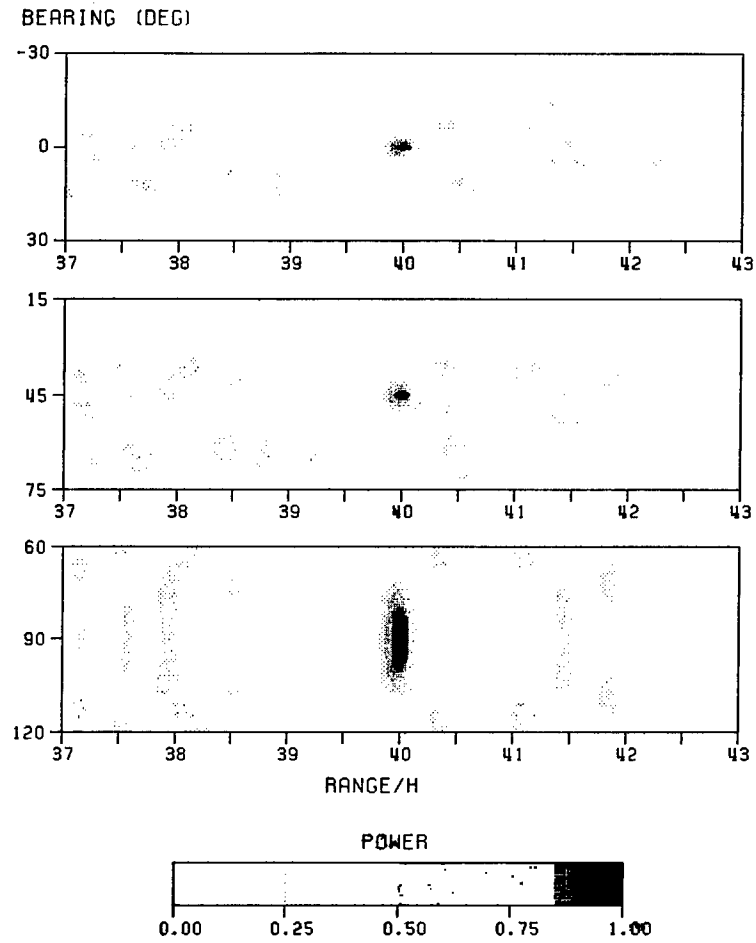


Fig. 7 — Range-bearing ambiguity surfaces for array with 45° tilt. Other parameters are as in Fig. 5. Array gain enhancement factors are 4.10 dB (top), 3.70 dB (middle), and 4.55 dB (bottom).

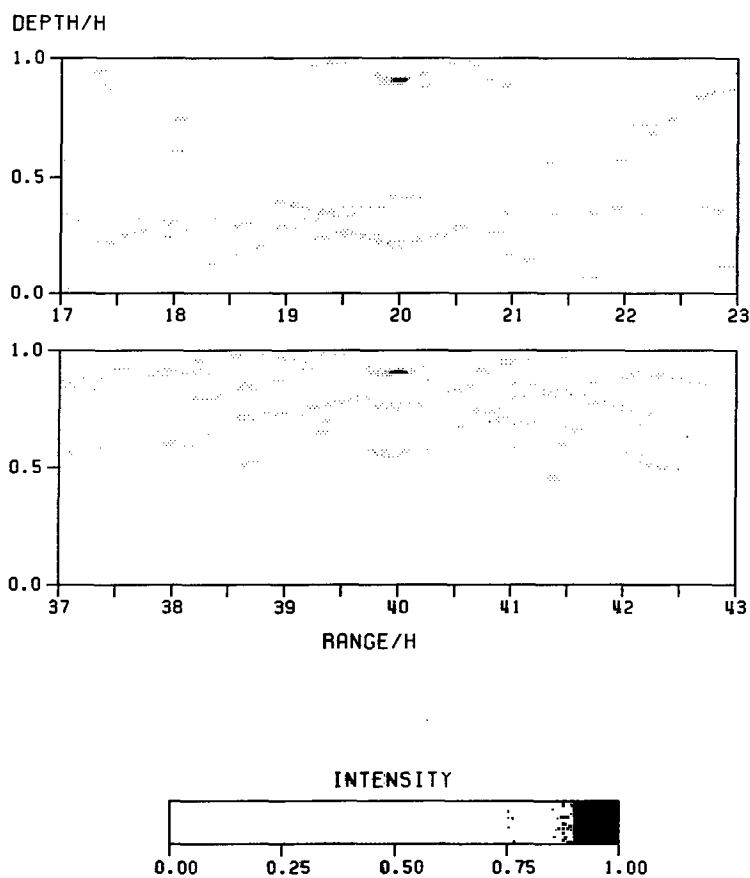


Fig. 8 — Range-depth ambiguity surfaces for vertical array, sources at distances 40 H (top) and 20 H (bottom). Array gain enhancement factors are 21.5 dB (top) and 21.3 dB (bottom).

Table 1 — Array Gain Enhancement and Range Resolution

Array (deg)	Target Bearing (deg) (or Range (H/λ))	Array Gain Enhancement (dB)	Range Spread of Main Peak (H/λ)
0	0	0.006	...
0	45	0.6	0.15
0	90	0.815	0.14
10	0	1.72	0.3
10	45	1.56	0.33
10	90	1.76	0.37
45	0	4.10	0.1
45	45	3.70	0.1
45	90	4.55	0.1
90	40	21.5	0.12
90	20	21.3	0.16

The results are obtained for an array of 31 hydrophone elements with an acoustic length of 20λ (one-third the water depth) and four array vertical tilt angles: 90° , 45° , 10° , and 0° . For the 90° tilt angle the array is vertical, so that the ambiguity surface depends only on the range and depth. For the 45° and the 10° vertical tilt angles, the array has horizontal extent (for 0° the array is purely horizontal), so that the ambiguity surface depends on source bearing as well as range and depth. For these cases, only the range-bearing slice corresponding to the exact source depth is shown. The ambiguity surfaces are normalized by the average intensity of the observed pressure field with the result that values range between zero and one. The unity value occurs at the true value of the source location parameter, as is shown analytically in the second section of this report and Appendix A. The array gain enhancement factors are obtained by averaging the maximum plane-wave beamformer response as the true source range varies over the same range interval as the corresponding ambiguity surface; they are listed in Table 1.

An inspection of the ambiguity surface for the purely horizontal array (Fig. 5), shows that increasing the source bearing can significantly reduce the range spread of the main lobe at the expense of introducing large extraneous sidelobes and increasing the azimuthal spread of both the main lobe and the sidelobes. The surface for broadside incidence (0° source bearing) has the power concentrated in a main lobe that has a modest azimuthal spread, but a range spread that exceeds the total, 6-channel-depth, range interval shown. In particular, for 0 azimuth the peak of the ambiguity surface lies within 0.02 of the maximum value of unity over the total range interval shown. In contrast, the surfaces for off-broadside incidence (45° and 90° source bearings) show the power concentrated in a main lobe with a dramatically reduced range spread and in four large sidelobe distributed along the range axes at an azimuth corresponding to the true source bearing. For the 45° source bearing, the range spread of the main lobe is only about $0.31 H/\lambda$, and the levels of the extraneous sidelobes are approximately 0.95. For the 90° source bearing, both the range spread of the main lobe and the levels of the sidelobes are slightly smaller. Also note that the azimuthal spread of both the main lobe and the sidelobes has increased to about 31° . Figure 5 suggests that, for the purely horizontal array, high-quality estimates of range, as well as bearing, could be obtained for sources off broadside, but only under very high S/N conditions. This is because the very small range spread of the main lobe determines the accuracy of the range estimate only when a sidelobe peak is not confused with the mainlobe peak. When S/N is small enough, so that a sidelobe peak exceeds the mainlobe peak a large percentage of the time, significant range errors can result.

Figures 6 and 7 show the ambiguity surface for array tilts of 10° and 45° , and the same set of source bearing angles as those for the purely horizontal array. Two features are evident in an inspection and comparison of these two figures. First, as is the case for the horizontal array, as the source bearing increases, the power becomes concentrated in the main lobe and in sidelobes distributed along the range axes, and the azimuthal spread of both the main lobe and the sidelobes increases. Secondly, increasing the array tilt can decrease the range spread of the mainlobe and decreases both the range spread and the level of the extraneous sidelobes. As specific examples, for sources off broadside, the range spread decreases from about $0.31 H/\lambda$ for 0° array tilt to about $0.21 H/\lambda$ for a 45° tilt. Furthermore, for the 10° array tilt, the largest sidelobe peak is approximately 0.85, with typical values of about 0.55; for the 45° array tilt, the largest sidelobe peaks are about 0.5, and typical values are about 0.3.

Bearing resolution, as measured by the azimuthal spread of each main lobe in Figs. 5 through 7, in most cases is found to be larger than, but roughly comparable to, the theoretical resolution of a conventional beamformer for a planewave signal incident on that array. The mainlobe spread is not strongly dependent on array tilt, as can be seen for a source at 45° , for which mainlobe spread is about 6° to 7° for all arrays. Sidelobe are distributed over wider azimuths for increased tilt angles; however, the reduction in sidelobe peaks compensates for the wider distribution, and source localization is enhanced for increased array tilt in all cases. For each geometry, conventional beam patterns were averaged over the range interval to obtain a measure of comparison of angular resolution, and in most cases the ambiguity surface resolution was superior to the conventional. Table 2 presents these results.

Table 2 — Angular Resolution

Array Tilt (deg)	Target Bearing (deg) or Range (H/λ)	Azimuth Spread (deg) or Depth Spread (H/λ) of Main Peak	Azimuth Spread of Averaged Conventional (deg)
0	0	2.8	2.5
0	45	6.4	4.6
0	90	31.4	38.
10	0	7.4	7.2
10	45	7.4	8.2
10	90	25.0	30.0
45	0	4.6	multiple peaks spread over 22°
45	45	6.4	multiple peaks spread over 36°
45	90	31.4	multiple peaks spread over 42°
90	40	0.0125	N/A
90	20	0.0125	N/A

Several features can be noted in Fig. 8, which shows range-depth ambiguity surfaces for a vertical array with sources at ranges of $40 H/\lambda$ and $20 H/\lambda$. First, for both sources, the range spreads of the main peaks are comparable to those for the array with 45° tilt, and at the true sources depth the largest sidelobes are below 0.5, with few exceeding 0.25. Secondly, the depth spreads of the main peaks are about $0.03 H/\lambda$ for both ranges, and most sidelobes which exceed 0.5 at other depths are at ranges close to the main lobe. Thus as the vertical extent of the array increases, range estimation is improved both by a general narrowing of the main peak and by reducing ambiguous sidelobes at other ranges; at the limit of a purely vertical array, excellent range accuracy is achieved for the Pekeris channel, with a highly localized main peak and few spurious sidelobes.

CONCLUSIONS AND RECOMMENDATIONS

The results of this study suggest that for acoustic fields with a complex arrival structure, with power spread over a significant vertical angle among a number of *multipaths*, ambiguity function processing can result in both high-quality estimates of the source location and a significant improvement in S/N relative to conventional beamforming. For arrays with minimal vertical tilt, a small improvement in array gain over conventional beamforming can be achieved, with improved bearing estimation for targets off broadside. Range estimates can be affected by broad mainlobe peaks and the presence of numerous sidelobes.

As the vertical tilt angle increases, the array gain enhancement over a conventional beamformer is increased, and the range spread of the main peak may be reduced for all source bearings, while small azimuthal spreading of the main peak is retained. Increased tilt also significantly reduces the level of the sidelobe peaks, which has major implications on the ability to estimate source range as well as bearing, by resolving range and bearing ambiguities present with shallower tilt angles.

Ambiguity surface processing with vertical array segments is found to provide depth estimates which are highly localized, with narrow main peaks and low sidelobe structures. More study is necessary to determine the degree of vertical extent necessary to achieve good depth discrimination.

These results suggest that, for complicated acoustic field cases, estimating source range as well as bearing requires apertures with significant (somewhat in excess of five wavelengths) vertical array extent. It can be shown that, with a significant vertical extent, high range resolution of the main peak can be achieved at average S/Ns on the order of 0 dB.

It is emphasized that the results presented here do not constitute a thorough performance analysis. For the Pekeris channel, there has been no attempt to determine the dependence of the performance on the ratios of bottom-to-water densities, water-to-bottom velocities, or depth-to-wavelength, nor on the length of the array segment. Nor has there been an investigation of the sensitivity of the estimates to uncertainties in knowledge of the environment; i.e., a mismatch between the actual field structure and the structure of the replica fields.

Further study is needed to quantify these performance indices and to apply the ambiguity surface processor to other acoustic environments.

ACKNOWLEDGMENTS

We acknowledge the assistance of Bruce Pasewark for suggestions to improve the programs used to produce the displays here, Orest Diachok for suggestions to clarify several sections of this report, and the Office of Naval Research for supporting this work.

Appendix A
MAXIMUM ARRAY GAIN VALUE

Equation (3) is established by showing that, for spatially uncorrelated noise fields, the noise gain is

$$GN = (1/N), \quad (\text{A1})$$

and, for an arbitrary set of replica functions $|s_n\rangle$, the signal gain satisfies

$$GS \leq 1, \quad (\text{A2})$$

with equality if, and only if, the replica field is proportional to the observed pressure field. Equation (A1) follows from Eq. (2c), since $E\{A \mid \text{noise only}\} = (E\{|p_n|^2 \mid \text{noise only}\})/N$ when the pressure field is spatially uncorrelated noise. Equation (A2) follows, since, according to the Cauchy-Schwartz inequality,

$$A \leq \left(\sum |p_n|^2 \right) \left(\sum |s_n|^2 \right) / \left(N \sum |s_n|^2 \right),$$

with equality if and only if $s_n = C \cdot p_n$ for some complex constant C . Equation (3) then follows from the assumption that the set of replica functions includes the observed pressure field.

Appendix B
MODAL FUNCTIONS, HORIZONTAL WAVENUMBER
COMPONENTS, AND THE NUMBER OF MODES

It is shown in Guthrie^{B1} that the modal functions are given by

$$U_m(z) = A_m \sin(G_m z/H), \quad (B1)$$

where

$$A_m = [(2/H)^{1/2} G_m] \quad (B2)$$

and the G_m are determined by

$$\tan(G_m) = - (G_m/\rho)/p[b^2 - G_m^2]^{1/2}, \quad (B3a)$$

where

$$b = (2\pi H/\lambda)[1 - c_r^2]^{1/2}. \quad (B3b)$$

Furthermore, the horizontal wavenumber components are

$$K_m = \hat{K}_m/\lambda, \quad (B4a)$$

where

$$\hat{K}_m = 2\pi [1 - ((G_m/H)/(2\pi/\lambda))^2]^{1/2}, \quad (B4b)$$

and the number of modes is

$$M = [(2H/\lambda)(1 - c_r^2)^{1/2}], \quad (B5)$$

where $[x]$ is the largest integer less than x .

The parameterization used in this report is established by noting that G_m , \hat{K}_m , and M depend only on c_r, ρ , and H/λ ; $z = z/H = (z/\lambda)/(H/\lambda)$; and $r \cdot K_m = (r/\lambda)\hat{K}_m$.

^{B1} M. Guthrie, "The Properties of SOFAR Signals," Ph.D. thesis, University of Auckland, 1974.

Appendix C IMPOSSIBILITY OF RESOLVING VERTICAL ARRIVAL STRUCTURE

The vertical arrival structure is obtained by expressing the sinusoid in Eq. (B1) as a sum of exponentials and substituting into Eq. (7). The result describes a pressure field consisting of the sum of M pairs of exponential functions, each pair representing cylindrical wavefronts of the form $\exp [i(K_m r \pm (G_m/H)z)]$. It follows from Eq. (B4) that the vertical arrival angles associated with each pair of wavefronts, ϕ_{vm} , satisfy

$$\sin(\phi_{vm}) = \pm (\lambda/2H)(m - (g_m/\pi)), \quad (C1a)$$

and total angular spread, $\phi_{vt} = |\phi_{v,M} - \phi_{v,-M}|$, is given by

$$\phi_{vt} = 2 \sin^{-1} [(\lambda/2H)(M - (g_M/\pi))], \quad (C1b)$$

where g_m is determined by

$$g_m = m\pi - G_m. \quad (C2)$$

From (B.3), it is seen that $g_m < g_{m+1}$, and that $g_m \in [0, \pi]$. Consequently,

$$M - (g_M/\pi) > (M - 1) > (2H/\lambda) \left[1 - c_r^2 \right]^{1/2} - 2,$$

so that ϕ_{vt} satisfies

$$\phi_{vt} > 2 \sin^{-1} [(1 - c_r^2)^{1/2} - (\lambda/H)]. \quad (C3)$$

To show that it is not possible to resolve the individual planewaves, we first note that the successive vertical arrival angles satisfy

$$\sin(\phi_{v,m}) - \sin(\phi_{v,m-1}) = (\lambda/2H) [1 - (g_m - g_{m-1})/\pi], \quad (C4)$$

so that

$$\sin(\phi_{v,m}) - \sin(\phi_{v,m-1}) < (\lambda/2H), \quad (C5)$$

since $[g_m]$ is a positive increasing sequence. The result then follows since the zeros in the beam pattern of an array of length L satisfy

$$\sin(\phi_k) - \sin(\phi_{k-1}) = (\lambda/2L), \quad (C6)$$

and L can not exceed H .

REFERENCES

1. Bucker, H.P. "Use of Calculated Sound Fields and Matched-Field Detection to Locate Sound Sources in Shallow Water," J. Acoust. Soc. Am., Vol. 59, p. 368, 1976.
2. Guthrie, M. "The Properties of SOFAR Signals," Ph.D. thesis, University of Auckland, 1974.